Wall attraction and repulsion of hydrodynamically interacting particles

Steffen Schreiber[1], Jochen Bammert[1], Philippe Peyla[2] and Walter Zimmermann[1]
[1] *Theoretische Physik I, Universität Bayreuth, 95440 Bayreuth, Germany and*
[2] *Laboratoire Interdisciplinaire de Physique, UMR,*
Université Joseph-Fourier, 38402 Saint Martin d'Heres, France
(Dated: June 8, 2012)

We investigate hydrodynamic interaction effects between colloidal particles in the vicinity of a wall in the low Reynolds-number limit. Hydrodynamically interacting pairs of beads being dragged by a force parallel to a wall, as for instance during sedimentation, are repelled by the boundary. If a pair of beads is trapped by harmonic potentials parallel to the external flow and at the same distance to a wall, then the particle upstream is repelled from the boundary while its neighbor downstream is attracted. The free end of a semiflexible bead-spring polymer-model, which is fixed at one end in a flow near a wall, is bent towards the wall by the same reason. The results obtained for point-like particles are exemplarily confirmed by fluid particle dynamics simulations of beads of finite radii, where the shear induced particle rotations either weaken or enhance the effects obtained for point-like particles.

I. INTRODUCTION

The flow properties of suspensions depend very much on the interaction between particles via the fluid, the so-called hydrodynamic interaction (HI) [1–4]. In microfludics, where the distance between particles and walls becomes often small, the dynamics of particles can be strongly influenced by the wall-induced hydrodynamic interaction effects between rigid as well as for soft particles, such as vesicles or polymers. Accordingly, particles may experience displacements across the unperturbed streamlines of an external flow and therefore, may lead to particle redistributions across the pipe diameter, if HI and inertia effects are taken into account. Thus, studies of suspensions are essential both from the fundamental and from the practical point of view.

In the case of small but finite values of the Reynolds number, Segré and Silberberg discovered the effect of cross-stream migration of particles to specific positions away from the centerline of a tube flow [5–10]. This particle focusing is understood to arise from the force balance between a wall effect that drives the particles to the center of a channel and a shear-gradient-induced migration pushing the particles towards the boundary.

In the over-damped Stokes limit in fluid dynamics the interplay between the HI and the deformability of soft particles like tank-treading vesicles in shear flows leads to a lift force close to boundaries [11–13]. For single soft particles such as oil drops or vesicles, their deformability combined with the shear gradient in Poiseuille flow causes cross-stream migration [7, 14], even in the absence of wall effects. In these cases the interesting question arises, whether and to which extend particle-wall HI affects the cross-streamline migration too [15]. Wall-induced cross-stream migration may occur also for polymers in suspension in a pipe flow, which is a long studied and important problem with a number of recent insights [16–20], or during sedimentation [21] with particle depletions close to a boundary [22] and during active motions of microswimmers in confinement [23]. Moreover, it has been found experimentally and theoretically that swimming microorganisms may be attracted by solid walls [24].

Wall-grafted polymer-brushes, which are also used for tuning surface properties in microchannels, are another example [25–27], where the particle-wall interactions play an important role for the dynamics of polymers and which differs significantly from that in the bulk. For instance, the cyclic motion of polymers tethered at a surface depends crucially on the interplay between the polymer-wall interaction and the shear flow [28–34]. Here, the HI plays a major role similar as for the related oscillatory motion of three trapped and hydrodynamically interacting particles in shear flow [35]. A related problem is the dynamics of cellulose fiber suspensions close to a wall, which is important for paper-manufacturing and therefore intensively investigated in order to better control the fiber orientation [36].

The examples mentioned so far focus mainly on the behavior of single rigid or soft particles (with more dynamical degrees of freedom) in fluid flow. For several disconnected particles there are a number of other interesting hydrodynamically induced interaction effects even in the bulk and in the absence of fluctuations. Besides the oscillatory dynamics of three sedimenting free particles [37] and of three trapped particles in shear flow [35], one finds also HI induced attraction or repulsion between asymmetric rotors [38], and an attraction between tethered polymers in plug flow [39]. For a diluted suspension of Brownian particles in shear flow an enhanced self-diffusion in shear flows is reported [40], which is explained by a wall-induced migration of free particles [41].

In this work we focus on boundary induced hydrodynamic interaction effects between particles fixed closed to a wall in Stokes flow or dragged particles in a quiescent fluid as described by the well known technique introduced by Blake for point particles [42] (whereof extensions may be found for instance in Refs. [17, 43, 44]). The reminder of the article is organized as follows: The related basic equations of motion for point-like particles are presented in Sec. II, including a summary of Blake's

results. The results of our numerical and analytical investigations on the particle-wall HI are presented in Sec. III, where as a basis of our analysis the flow lines around a single particle close to a wall are given in Sec. III A. Two or more sedimenting particles near a boundary are considered in Sec. III B, where a cross-streamline migration away from the wall can be qualitatively explained in terms of the flow lines around a single particle. The case of two trapped point like particles exposed to a flow is described in Sec. III C. The results of the two trapped particles are qualitatively confirmed by fluid particle dynamics simulations [45, 46] for particles with finite radii and they illustrate the major effects that are relevant for the applications to semiflexible bead-spring models in Sec. IV. In Sec. IV A a semiflexible bead-spring chain tethered close to a wall and exposed to a flow is treated and in Sec. IV B semiflexible polymers perpendicularly anchored at a wall in shear flow. The article closes in Sec. V with a discussion of the results and suggestions of possible experiments.

II. MODEL EQUATIONS

We consider the dynamics of colloidal particles in the limit of a vanishing Reynolds number, where the laminar flow is described by the Stokes equation for an incompressible Newtonian fluid. If not stated otherwise we assume point-like particles with an effective hydrodynamic radius a.

The dynamics of the N beads at the positions $\mathbf{r}_i$ ($i = 1, \ldots, N$) is governed by N coupled equations

$$\dot{\mathbf{r}}_i = \mathsf{H}_{ij}\mathbf{F}_j + \mathbf{u}_0(\mathbf{r}_i)\,, \tag{1}$$

where $\mathbf{u}_0(\mathbf{r}_i)$ is an externally applied flow as for example a linear shear flow

$$\mathbf{u}_0(\mathbf{r}) = u_0(z)\hat{\mathbf{x}} = \dot{\gamma} z \hat{\mathbf{x}}\,, \tag{2}$$

with the shear rate $\dot{\gamma}$. The force $\mathbf{F}_j$ is the sum over all potential forces acting on the j-th bead. Depending on the specific system, these may include stretch or bending forces as well as forces due to trap potentials, which can be derived from a potential V according to

$$\mathbf{F}_j = -\nabla_j V, \tag{3}$$

where ∇_j denotes the gradient with respect to $\mathbf{r}_j$. The relevant expressions for V are specified in Sec. III and Sec. IV.

H_{ij} refers to the mobility matrix describing the HI between the beads i and j. In the presence of a plane wall with a no-slip boundary condition for the fluid at the wall, H_{ij} is given by the Blake tensor [42],

$$\begin{aligned}\mathsf{H}_{ij}(\mathbf{r}_i, \mathbf{r}_j) = {}& {}^{S}\mathsf{H}_{ij}(\mathbf{r}_i, \mathbf{r}_j) - {}^{S}\mathsf{H}_{ij}(\mathbf{r}_i, \mathbf{r}'_j) \\ & + {}^{D}\mathsf{H}_{ij}(\mathbf{r}_i, \mathbf{r}'_j) - {}^{SD}\mathsf{H}_{ij}(\mathbf{r}_i, \mathbf{r}'_j)\,,\end{aligned} \tag{4}$$

where $\mathbf{r}'_j = (x_j, y_j, -z_j)$ is the position of the mirror image of bead j at the opposite side of the boundary. The first contribution to H_{ij} accounts for the HI in the unbounded domain described by the Oseen tensor [3],

$${}^{S}\mathsf{H}_{ij}^{\alpha\beta}(\mathbf{r}_i, \mathbf{r}_j) = \begin{cases} \frac{1}{8\pi\eta r_{ij}}\left(\delta_{\alpha\beta} + \frac{r_{ij}^{\alpha} r_{ij}^{\beta}}{r_{ij}^2}\right) & \text{for } i \neq j\,, \\ \frac{1}{6\pi\eta a}\,\delta_{\alpha\beta} & \text{for } i = j\,, \end{cases} \tag{5}$$

and the second one for the HI between the beads and their mirror images,

$${}^{S}\mathsf{H}_{ij}^{\alpha\beta}(\mathbf{r}_i, \mathbf{r}'_j) = \frac{1}{8\pi\eta\tilde{r}_{ij}}\left(\delta_{\alpha\beta} + \frac{\tilde{r}_{ij}^{\alpha}\tilde{r}_{ij}^{\beta}}{\tilde{r}_{ij}^2}\right)\,, \tag{6}$$

where η is the viscosity of the fluid. We furthermore use the abbreviations

$$\mathbf{r}_{ij} = \mathbf{r}_i - \mathbf{r}_j = r_{ij}\hat{\mathbf{r}}_{ij}\,, \tag{7a}$$

$$\tilde{\mathbf{r}}_{ij} = \mathbf{r}_i - \mathbf{r}'_j = \tilde{r}_{ij}\hat{\tilde{\mathbf{r}}}_{ij} \tag{7b}$$

and the components of the vector $\mathbf{r}_{ij}$ ($\tilde{\mathbf{r}}_{ij}$) are denoted by r_{ij}^{α} ($\tilde{r}_{ij}^{\alpha}$), where $\alpha = x, y, z$. In Eq. (4) the contribution

$${}^{D}\mathsf{H}_{ij}^{\alpha\beta}(\mathbf{r}_i, \mathbf{r}'_j) = \frac{1}{4\pi\eta\tilde{r}_{ij}^3}\, z_j^2(1 - 2\delta_{\beta z})\left(\delta_{\alpha\beta} - 3\frac{\tilde{r}_{ij}^{\alpha}\tilde{r}_{ij}^{\beta}}{\tilde{r}_{ij}^2}\right) \tag{8}$$

is the Stokes doublet (D) and

$$\begin{aligned}{}^{SD}\mathsf{H}_{ij}^{\alpha\beta}(\mathbf{r}_i, \mathbf{r}'_j) = {}& \frac{1}{4\pi\eta\tilde{r}_{ij}^3}\, z_j(1 - 2\delta_{\beta z}) \\ & \left(\delta_{\alpha\beta}\tilde{r}_{ij}^{z} - \delta_{\alpha z}\tilde{r}_{ij}^{\beta} + \delta_{\beta z}\tilde{r}_{ij}^{\alpha} - 3\frac{\tilde{r}_{ij}^{\alpha}\tilde{r}_{ij}^{\beta}\tilde{r}_{ij}^{z}}{\tilde{r}_{ij}^2}\right)\end{aligned} \tag{9}$$

is the source doublet (SD). In our numerical calculations higher order corrections to H_{ij} due to the finite size of the spheres are included up to the order a^2 (Rotne-Prager approximation). The final equations of motion are given by

$$\dot{\mathbf{r}}_i = \tilde{\mathsf{H}}_{ij}\mathbf{F}_j + \mathbf{u}_0(\mathbf{r}_i)\,, \tag{10}$$

where the mobility matrices

$$\tilde{\mathsf{H}}_{ij} = \left(1 + \frac{a^2}{6}\nabla_i^2 + \frac{a^2}{6}\nabla_j^2\right)\mathsf{H}_{ij} \tag{11}$$

fulfill the relation $\mathsf{H}_{ij} = \mathsf{H}_{ji}^{\mathsf{T}}$, which is important for the overall symmetry of the problem - as pointed out in Ref. [44].

III. RESULTS FOR BASIC MODELS

In this section we determine the influence of wall-induced hydrodynamic interactions on the dynamics of two and three beads which are either dragged in a fluid parallel to a boundary or hold in potentials near a wall and exposed to flows. To this end Eq. (10) with Eq. (11) is solved numerically for the viscosity $\eta = 1$ and approximate analytical solutions are given in some cases.

A. A single trapped bead in shear flow close to a wall

The influence of a wall on the HI between two beads can be illustrated by the streamlines around one point-like particle with an effective hydrodynamic radius a at a distance d_w from a solid boundary. The particle is exposed to the flow given by Eq. (2) and is trapped by a harmonic potential

$$V = \frac{k_{\rm pot}}{2}(\mathbf{r}_b - \mathbf{r}_{\rm pot})^2\,, \tag{12}$$

where $\mathbf{r}_b$ is the position vector of the particle, $\mathbf{r}_{\rm pot}$ the position of the potential minimum, with a spring constant of $k_{\rm pot} = 1$. Equivalently, one could consider a point-like particle dragged by a constant external force $\mathbf{F} = f\hat{\mathbf{x}}$ parallel to the wall in a quiescent fluid. The streamlines around the point-like particle are the same in both cases if a comoving frame is chosen, where the particle's position is held fixed by the potential at $\mathbf{r}_{pot} = (0, 0, d_w)$.

The trap force $\mathbf{F}^s = -k_{\rm pot}\,(\mathbf{r}_b - \mathbf{r}_{\rm pot})$ as a function of the unperturbed flow velocity $\mathbf{u}_0(\mathbf{r})$ is obtained by solving Eq. (10) for a vanishing bead velocity $\dot{\mathbf{r}}_b = 0$:

$$0 = \tilde{\mathsf{H}}(\mathbf{r}_b, \mathbf{r}_b)\mathbf{F}^s + \mathbf{u}_0(\mathbf{r}_b)\,. \tag{13}$$

We find for the Oseen approximation

$$F_x^s = f_x\,\frac{16d_w}{16d_w - 9a} \qquad \text{and} \qquad F_y^s = F_z^s = 0\,, \tag{14}$$

with $f_x = -6\pi\eta a u_0(d_w)$ the force required to keep the particle fixed in the absence of a wall, if it is exposed to a flow with the velocity $u_0(d_w)$. When $u_0(d_w)$ is constant for varying d_w, *e.g.*, by adjusting the shear rate appropriately, the force F_x^s exerted on the bead increases with decreasing d_w. This effect will be investigated further in subsection III C.

The vanishing force $F_z^s = 0$ perpendicular to the wall in Eq. (14) reflects the time reversibility of the Stokes equation [1]. If a single bead in shear flow would migrate perpendicularly to the wall, *i.e.* $F_z^s \neq 0$, then for symmetry reasons the drift would point in the same direction after reversing the flow. But then the motion would not be reciprocal and the time-reversibility of the Stokes equation would be violated. Therefore, $F_z^s \neq 0$ is forbidden and there is no migration of a single bead perpendicular to the wall.

The flow field $\mathbf{u}(\mathbf{r})$ around a bead fixed at $\mathbf{r}_b = (0, 0, d_w)$ shown in Fig. 1 is given by

$$\mathbf{u}(\mathbf{r}) = \left(1 + \frac{a^2}{6}\Delta\right)\mathsf{H}(\mathbf{r}, \mathbf{r}_b)\mathbf{F}^s + \mathbf{u}_0(\mathbf{r})\,. \tag{15}$$

In the absence of a boundary, where only the first contribution in Eq. (4) has to be taken into account, the streamlines are up/down and left/right symmetric with respect to the center of the bead. In the presence of a wall this up/down symmetry is broken and the streamlines are deformed as indicated in Fig. 1. This effect is caused by the HI between the fixed bead and the boundary, which is described by the second, third, and fourth contribution to the mobility matrix in Eq. (4).

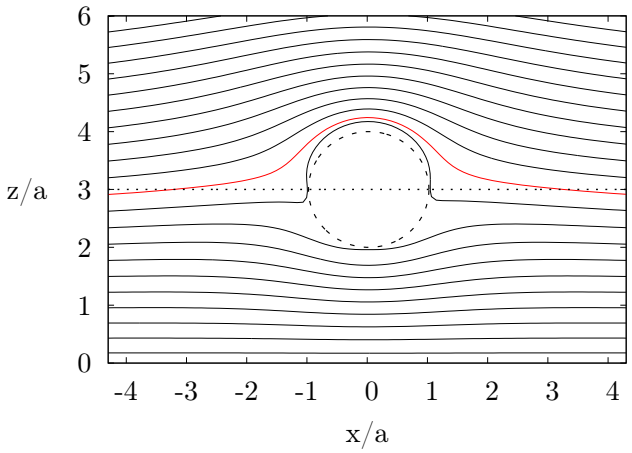

FIG. 1. In the xz plane the streamlines around the bead fixed at $\mathbf{r}_b = (0, 0, d_w = 3)$ are in the presence of a plane no-slip boundary at $z = 0$ asymmetric with respect to the axis at $z = d_w$. One obtains the same asymmetry of the flow lines in the co-moving frame of a point particle dragged parallel to the boundary along the dotted line at $z = d_w$. The flow lines were calculated via Eq. (15), whereby the red line marks the trajectory of a test particle starting and terminating below the center of the bead but passing the bead on top.

If one introduces a small tracer particle, starting at $x < 0$ at a height $z < d_w$, it follows one of the displayed streamlines as indicated by the red streamline in Fig. 1 and may pass the bead at the side opposite from the wall, *i.e.* $z > d_w$. According to the $\pm x$ symmetry the streamline reaches the range $z < d_w$ again for large x. This is a consequence of the time-reversibility of the Stokes equation, which is also valid in the presence of a solid boundary. The wall-induced deformation of the streamlines has interesting consequences as discussed in the following sections.

B. Particles dragged parallel to a boundary - a model for sedimentation

Here we investigate the motion of several particles which are dragged by a constant external force $\mathbf{F}$ parallel to a wall, as for example by the gravitational force during the sedimentation of particles.

We first consider the motion of two beads dragged in an unbounded fluid. If the force $\mathbf{F}$ acts parallel or perpendicular to the connection vector between both particles, $\mathbf{r}_{12} = \mathbf{r}_1 - \mathbf{r}_2$, cf. Fig. 2(a) and (b), they move in either case parallel to the force, as indicated in Fig. 2 by part a) and b). If $\mathbf{r}_{12}$ encloses an angle $\Theta \neq 0$ and $\Theta \neq \pi/2$ with the force $\mathbf{F}$, the particles move obliquely with re-

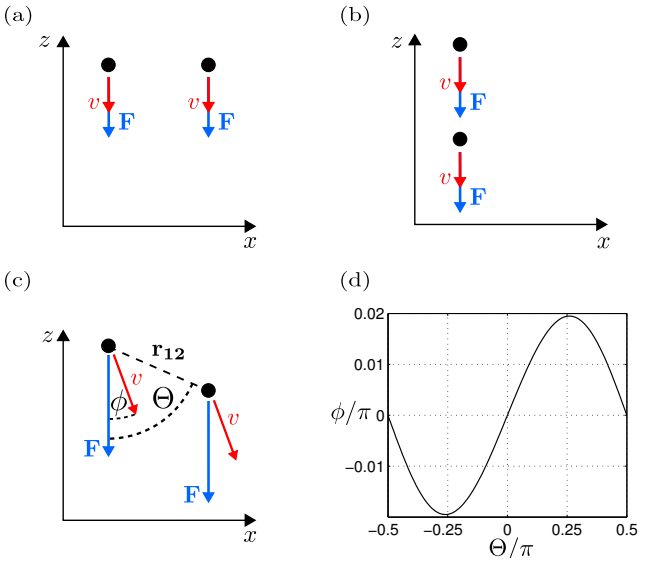

FIG. 2. Two particles are dragged through a fluid by a force **F** anti-parallel to the vertical z axis. The beads move parallel to **F**, if the connection vector $\mathbf{r}_{12}$ encloses with **F** an angle $\Theta = \pi/2$, as in part (a), or $\Theta = 0$, as in part (b). For other values of Θ the HI effects cause an angle ϕ between the direction of the particle velocity **v** and **F**, as indicated in (c) [48]. An approximation of the dependence of ϕ on Θ is given by Eq. (16) and plotted in (d).

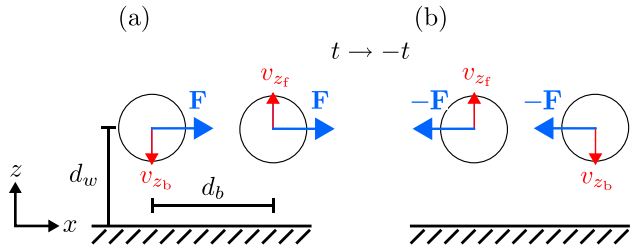

FIG. 3. Each of the two beads in part a) is dragged by a force **F** parallel to a wall. The particle in front is repelled from the wall, while the bead behind is attracted, as expected by the form of the streamlines around a single bead in Fig. 1. In part b) the time has been reversed and thus the direction of the applied force and the particle motion are reversed too.

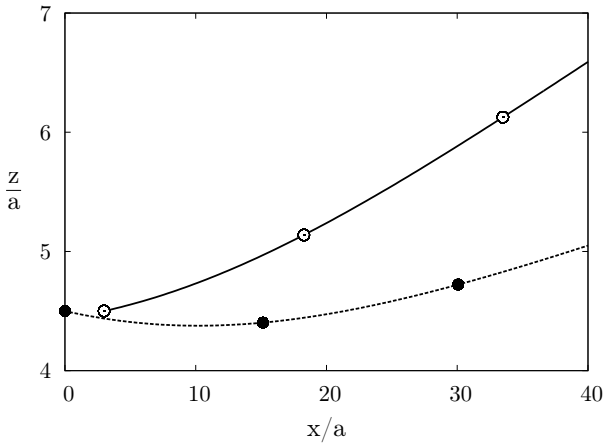

FIG. 4. The trajectories of two beads in the xz plane are shown, which are dragged through the fluid by an external force $\mathbf{F} \parallel \hat{\mathbf{x}}$ parallel to the boundary at $z = 0$. The initial positions of both beads are located at $\mathbf{r}_1 = (0, 0, d_w)$ and $\mathbf{r}_2 = (d_b, 0, d_w)$ with $d_b = 3a$ and $d_w = 4.5a$. The particle positions are indicated by open and filled circles along the trajectories at equal times. The bead behind (dashed line) is at first attracted towards the wall due to the wall-mediated HI, whereas the particle in front (solid line) is always repelled. Later on the bulk HI dominates and both particles move away from the wall, as expected according to Eq. (16).

spect to the drag force due to the HI between the beads as indicated in Fig. 2(c) (see also [48]). The deflection angle ϕ between the direction of the particle motion and the force has its maximum value at $\Theta = \pm\pi/4$ and is in the Oseen approximation given by

$$\phi = \arctan\left(\frac{\sin\Theta\cos\Theta}{1 + \frac{4d}{3a} + \cos^2\Theta}\right), \qquad (16)$$

where $d = |\mathbf{r}_{12}|$ is the distance between the particles.

In the presence of a boundary the particle-particle hydrodynamic interaction via the boundary comes into play. As already indicated by the flow lines around a single particle in Fig. 1, a wall breaks the symmetry around the particle with respect to the z direction. For two particles, which are initially located at the same distance from a wall and pulled parallel to it, as depicted in Fig. 3(a), we show in Fig. 4 the trajectories of point particle's determined numerically from Eq. (10). The open and the filled circles in Fig. 4 represent the particle positions at equal times.

The bead in front is repelled by the wall immediately from the start, while the particle behind is at first attracted to the wall, as indicated in Fig. 3a). Later on the rear bead moves away from the wall as well. In order to understand this effect it is useful to consider the early and the later stage of the motion shown in Fig. 4 for each particle. For the early regime the flow-lines around a single bead, as shown in Fig. 1, allow an estimate about the motion of the two particles along the z direction. In the front of a pulled particle the velocity of the fluid has a component in the positive z direction and in the negative z direction behind it. Accordingly, in the case of a pair of dragged beads the particle in front is repelled from the wall whereas the one behind is attracted towards the boundary as sketched in Fig. 3(a). During this process of wall-particle repulsion and attraction the connection vector $\mathbf{r}_{12}$ becomes skewly oriented to the drag force, i. e. $\Theta \neq 0$ as indicated in Fig. 2c), with the particle closer to the wall behind the other.

If the connection vector is skewly oriented, the bulk

effect, as described above, comes into play in the second stage of the motion. It causes in the case, when the particle closer to the wall moves behind the other one, a drift of both particles perpendicular to the external force and away from the wall. The bead closer to the wall moves slower than the other one because its effective friction is enhanced closer to the wall (cf. Eq. (14)) and therefore the bead distance d increases and Θ decreases. Consequently $|\phi|$ decreases in agreement with Eq.(16). In the long-time limit the particles' trajectories align with the applied forces, in which case the wall distance of both particles practically saturate. Therefore, the essential effect of the hydrodynamic particle-wall-particle interaction on the motion of the beads shown in Fig. 4 is the reorientation of their connection vector $\mathbf{r}_{12}$. When $\mathbf{r}_{12}$ is oblique to the drag force, the bulk effect provides the major contribution to the migration of the particles away from the wall.

Near a point-like particle at $\mathbf{r} = (0, 0, d_w)$, which is dragged parallel to a boundary, the induced velocity of the fluid around it can be determined analytically by taking the wall effects into account in the Oseen-approximation. In this case the non-zero z-component of the velocity of the fluid at the positions $\mathbf{r}_\pm = (\pm d_b, 0, d_w)$ is as follows:

$$v_{z_\pm} = \pm \frac{3}{2} \frac{f}{\pi\eta} \frac{d_b d_w^3}{(4d_w^2 + d_b^2)^{5/2}} \,. \qquad (17)$$

If a free test particle is placed at $\mathbf{r}_\pm$ near the dragged particle, it moves with the fluid and its induced vertical velocity component is given by the fluid velocity $v_{z_\pm}$. These velocity components have the same magnitude in the front and in the rear of the dragged particle, whereas they point in opposite directions as indicated also by the streamlines shown in Fig. 1. According to this qualitative reasoning one expects in the case of a pair of beads, which are dragged parallel to a wall, that the particle in front is repelled from the wall whereas the rear one is attracted towards the wall.

Eq. (17) displays also the reciprocity of trajectories in Stokes flow. If the time and therefore the direction of the applied forces are reversed, then in the discussed setup the bead in front is again repelled from the wall and the rear one is driven to the wall, as indicated in Fig. 3(b). After the time-reversal the role of the beads is interchanged, with $v_{z_+} = -v_{z_-}$ and the motion is reciprocal to the one before, thus obeying the time reversibility of the Stokes-equation.

Fig. 5 shows the trajectories of two particles as obtained by integrating Eq. (10) for two particles dragged by a force $\mathbf{F} \parallel \hat{\mathbf{x}}$ along a wall at $z = 0$ and interacting via the Rotne-Prager approximation. The bead connection vector $\mathbf{r}_{12}$ at the initial position encloses an angle $\Theta < \pi/2$ with $\mathbf{F}$. In this case, the bead closer to the wall, *i.e.* $z = 0$, is slightly in front of the other one, and due to the bulk effect described above (cf. Fig. 2), both beads first approach the wall. As the HI with the boundary and thus the friction becomes stronger the bead closer to the wall becomes slower than the more distant particle (cf. Eq. (14)). Consequently, the particle further from the boundary finally overtakes the other one and in this case $\mathbf{r}_{12}$ becomes again oblique with respect to $\mathbf{F}$ with $\Theta > \pi/2$ leading to a repulsion of both beads from the wall due to the bulk effect.

Besides the examples in Fig. 4 and Fig. 5 we investigated many other orientation angles between $\mathbf{r}_{12}$ and $\mathbf{F}$ ($\Theta = 0$, $\Theta = \pi/2$, $\Theta \gtrless \pi/2$). We obtain for all orientations of the connection vector finally a drift of both particles away from the wall. Hence, the wall-induced hydrodynamic particle-wall-particle interaction between two beads being dragged by a force parallel to a boundary eventually causes a repulsion of the particles from the wall for arbitrary initial conditions.

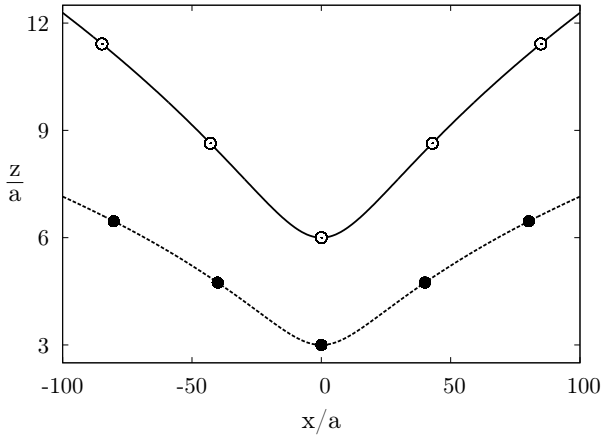

FIG. 5. The trajectories of two beads in the xz plane, which are dragged by an external force $\mathbf{F} \parallel \hat{\mathbf{x}}$ parallel to the boundary at the xy plane, *i.e.* $z = 0$. The initial bead connection vector $\mathbf{r}_{12}$ is slightly tilted with respect to the z axis so that the bead which is closer to the wall is slightly in front of the other one. The open and the filled circles visualize the positions of the two particles at equal times. First the beads approach the wall until the boundary effect causes a reorientation of $\mathbf{r}_{12}$, so that the particles are finally repelled from the wall.

The trajectories of three particles which are initially aligned perpendicularly to a wall are shown in Fig. 6. The initial distances between the beads and between the lowest particle and the wall are $3a$. As explained before, the bead which is furthest from the boundary is often slightly faster than the other two. Due to the bulk HI between the particles, which then have different x positions, the lowest and the highest bead perturb the flow in such a way that the middle particle experiences friction just as small as for the upper one. For the example in Fig. 6 the upper two particles finally build a pair and move away from the wall in a similar manner as in the case of two beads described above in Fig. 5, whereas the lower (third) particle moves similar to a single particle nearly parallel to the wall. For other initial

conditions similar formations of pairs of beads are found, which move finally away from the wall.

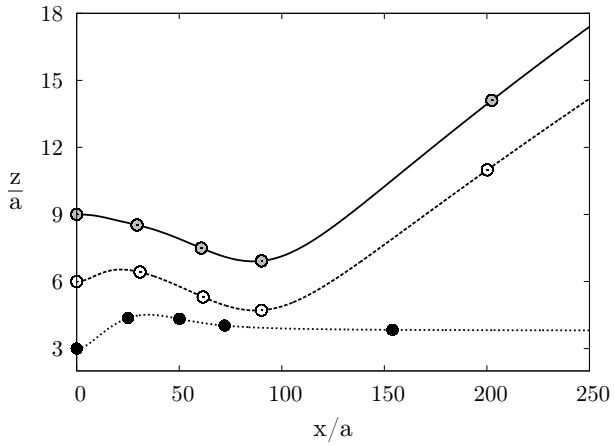

FIG. 6. The trajectories of three beads in the xz plane, which are dragged by an external force $\mathbf{F} \parallel \hat{\mathbf{x}}$ away from their initial positions: $(0, 0, 3a)$, $(0, 0, 6a)$ and $(0, 0, 9a)$. The positions of the particles at equal times are indicated by open, grey and black filled circles along the trajectories. Due to the interplay of bulk and wall HI effects the upper beads form a pair after an intermediate regime and finally drift away from the wall due to bulk HI effects. The third bead remains nearly at its initial distance from the wall.

The motion of an assembly of many particles is governed by the same principles as described above. By a complex interplay of bulk and wall effects pairs of beads form and dissolve, but the overall tendency is a migration of the particles away from the wall, similar to the results reported in Ref. [22], where the situation of small but finite values of the Reynolds number is investigated.

Another case, where the hydrodynamic particle-wall-particle interaction has to be considered, is when two beads are dragged perpendicularly to a wall with identical wall distances. This is equivalent to the situation of two sedimenting particles, when they approach the bottom boundary. In this case, the two beads repel each other slightly and the repulsion becomes significant at wall distances smaller than $10a$. Possible experimental setups for investigations of the effects predicted in this subsection are discussed in Sec. V.

C. Two trapped beads in shear flow close to a wall

In this section wall-induced HI effects are investigated for a system composed of two trapped particles in a linear shear flow near a wall. The harmonic trap potential is given by

$$V = \frac{k_{\mathrm{pot}}}{2} \left[(\mathbf{r}_1 - \mathbf{r}_{\mathrm{pot},1})^2 + (\mathbf{r}_2 - \mathbf{r}_{\mathrm{pot},2})^2 \right] , \qquad (18)$$

where $k_{\mathrm{pot}} = 1$ is the spring constant and $\mathbf{r}_1$ and $\mathbf{r}_2$ are the positions of the two beads. The locations of the potential minima are $\mathbf{r}_{\mathrm{pot},1} = (0, 0, d_w)$ and $\mathbf{r}_{\mathrm{pot},2} = (d_b, 0, d_w)$ with the connection vector $\mathbf{r}_{\mathrm{pot},1} - \mathbf{r}_{\mathrm{pot},2}$ parallel to the wall. The results discussed are obtained for point-like particles and compared to the case of finite-sized beads which undergo in addition shear-induced rotation.

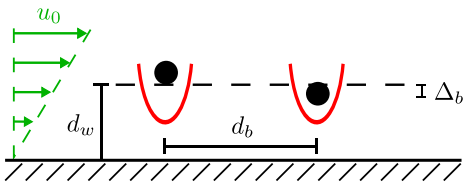

FIG. 7. Two point-like particles are trapped in a shear flow $\mathbf{u_0}(z)$ by harmonic potentials with their minima at a distance d_w from the wall at $z = 0$ and a mutual separation d_b. With the coordinate z_2 of the particle downstream $\Delta_b = d_w - z_2$ measures its displacement from the potential minimum.

The two point-like particles are displaced by the flow in x direction away from the minima of the trapping potential. Simultaneously, the wall-induced HI causes displacements along the z direction until the influence of the boundary is balanced by the potential forces. Similar to the previous section, the bead upstream is effectively repelled from the wall and the bead downstream is attracted. Note, that the deflection of the particle downstream is different from the displacement of the bead upstream, which is due to the bulk effect described in the previous subsection III B and can be explained as follows: Because of the finite angle Θ between the bead connection vector and the trap forces, cf. Fig. (2), both particles are shifted away from the wall. The boundary effect dominates, because the trap forces prevent the angle Θ from becoming too large, but due to the described shift the bead downstream is attracted towards the wall by a smaller distance than the one upstream is repelled from the wall.

The wall-induced particle displacement along the z direction is characterized by the shift

$$\Delta_b = d_w - z_2 \, , \qquad (19)$$

where z_2 is the steady-state position of the bead downstream.

In the following we determine the displacement Δ_b at the steady-state as a function of the flow velocity as well as of the distances d_w and d_b. As a first approach, Δ_b is approximated analytically for two point-like particles as shown in Fig. 7. The forces needed to hold the beads in place in an external flow can be estimated in a similar manner as described in Sec. III A, cf. Eq. (14). In the Oseen approximation their x components are given by

$$F_x^s = f_x \frac{16 d_b d_w}{8 d_w (2 d_b + 3a) - 9 a d_b} \qquad (20)$$

with $f_x = -6\pi\eta a u_0(d_w)$. For the particle downstream one obtains the initial velocity $v_{z\_}$ in z direction via Eq. (17) with $f = F_x^s$. The resulting Stokes force $F_z^s = 6\pi\eta a v_{z\_}$ can be used to estimate the elongation Δ_b in the steady state via the counteracting force $F_z^{\rm pot} = k_{\rm pot}\Delta_b$, which must fulfill $F_z^s + F_z^{\rm pot} = 0$. This calculation yields

$$\Delta_b = \frac{864\pi\eta a^2 d_b^2 d_w^4 u_0(d_w)}{k_{\rm pot}(4d_w^2 + d_b^2)^{5/2}\ [8d_w(2d_b + 3a) - 9ad_b]}\,. \quad (21)$$

Δ_b depends linearly on the unperturbed flow velocity $u_0(d_w)$, which itself increases linearly as a function of d_w according to Eq. (2). Since we are mainly interested in the d_w-dependence of the wall-induced HI effects and not in its dependence on the absolute value of $u_0(d_w)$, we adjust the shear rate according to the relation $\dot\gamma = u_0(d_w)/d_w$, such that the flow velocity $u_0(d_w)$ becomes independent of d_w:

$$\mathbf{u}_0 = u_0(d_w)\frac{z}{d_w}\,\hat{\mathbf{x}}\,. \quad (22)$$

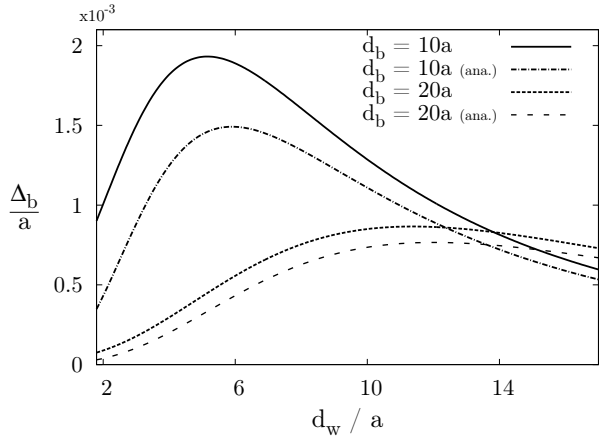

FIG. 8. The bead deflection Δ_b is plotted as a function of the wall distance d_w for two different distances $d_b = 10a,\ 20a$ between the potential minima, as indicated in Fig. 7, and for the flow field given by Eq. (22) with $u_0(d_w) = 0.004$. The dash-dotted line (second from above) and the dashed line (lowest one) correspond to the analytical approximations according to Eq. (21).

The analytical expression for Δ_b in Eq. (21) exhibits characteristic maxima as a function of d_w and as a function of d_b. The dependence of Δ_b on d_w is shown in Fig. 8 for the two different values $d_b = 10a,\ 20a$. In this figure the analytical results are compared with the numerically determined values, which were obtained via Eq. (10). Despite the assumptions included in Eq. (21), both curves agree with each other surprisingly well qualitatively, especially at larger distances d_w and d_b.

The maximum of $\Delta_b(d_w)$ in Fig. 8 can be traced back to Eq. (17), which represents the z component of the perturbed fluid velocity due to a dragged particle near a wall. This expression already exhibits a maximum as a function of d_w. However, for very large wall distances $d_w \gg d_b$ the influence of the boundary must vanish and Δ_b must approach 0. The dependence of Δ_b on

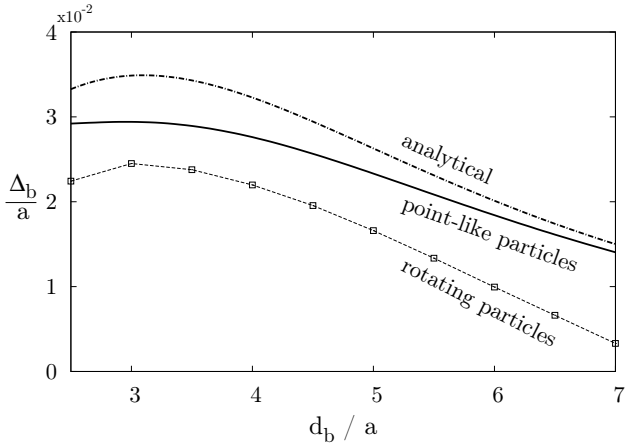

FIG. 9. Δ_b is plotted as a function of the bead distance d_b for the setup shown in Fig. 7 and Fig. 10. The distance to the wall is $d_w = 2.5a$ and the flow velocity is $u_0(d_w) = 0.004$. The solid line represents the results for point-like particles, where the effects of particle rotation are neglected. The squares are the result of simulations for particles of a finite size, which rotate in the external shear flow (cf. Fig. 10). The dash-dotted line is the result of the analytical approximation given by Eq. (21).

the particle-particle distance d_b is shown in Fig. 9 for $d_w = 2.5a$ and for the flow velocity $u_0(d_w) = 0.004$. The maximum of $\Delta_b(d_b)$ in the numerical solution (solid line), is less pronounced than in the corresponding analytical expression (dash-dotted line).

Up to this point we considered finite size effects of the particles up to second order in a (bead radius). Particles with a finite diameter also rotate in shear flows and therefore cause an additional contribution of third order, which is neglected. What is more, the rotation is also influenced by the vicinity of a wall [49, 50]. In order to quantify the influence of the rotation on the wall-induced HI and Δ_b, we performed computer simulations for finite-sized particles using the method of fluid particle dynamics (FPD) [45, 46]. In these simulations the particles are trapped in harmonic potentials at a distance $d_w = 2.5a$ to the wall and, as indicated in Fig. 10, they can freely rotate when exposed to a linear shear flow. In the FPD simulations for rotating particles the flow velocity at the particle positions $u_0(d_w) = 0.004$ is the same as in simulations of the point-like partiles. The squares in Fig. 9 represent the results from FPD simulations.

As displayed in Fig. 10 the shear flow profile in FPD

simulations was realized by moving the upper and the lower boundary into opposite directions by a constant velocity v_0. For such a configuration the shear induced particle rotation counteracts the effects of a wall (cf. Fig. 10). In spite of this counteraction the particle downstream is again effectively attracted to the wall and the particle upstream repelled, similar to the case of point-like particles. Accordingly, Δ_b is smaller for rotating particles than for point like particles of the same effective radius. In Fig. 7 and Fig. 10 the shear rates at the position of the particles have an opposite sign. This has for point like particles no influence on the elongation Δ_b. However, in FPD simulations of particles of a finite bead-diameter the bead rotations change their sign with the shear rate. In contrast to the case sketched in Fig. 10, shear induced bead rotations as indicated in Fig. 7 support the elongation Δ_b and Δ_b becomes in this case larger than for point like particles.

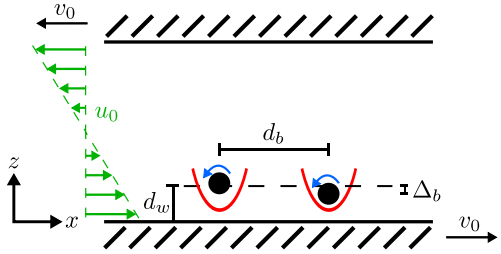

FIG. 10. The shear-induced particle rotation influences the wall-induced particle attraction and repulsion. For the given setup the deflection of both beads from their initial position $z = d_w$ is reduced due to the rotation effects. The influence of the rotational interaction is investigated exemplarily by fluid particle dynamics simulations of two trapped particles.

The shear rate in the FPD simulations was chosen such that the ratio between the difference of the flow velocity at the lower and at the upper side of the sphere, Δu_s, and the mean velocity $u_0(d_w)$ was $\frac{\Delta u_s}{u_0(d_w)} = \frac{2a\dot{\gamma}}{u_0(d_w)} = 0.37$. This causes a reasonably strong particle rotation and therefore a comparatively strong rotational HI. Despite this quite large ratio, the major contribution to Δ_b is caused by the wall-induced HI since $\Delta_b > 0$ (cf. Fig. 9). This result supports our approach to use point-like particles during the rest of this work for the analysis of the major trends of the wall-induced HI effects.

Δ_b becomes large for small values of d_b and d_w. In order to estimate Δ_b for possible experiments, we choose $d_b = 3a$ and $d_w = 2a$. Additionally, a typical potential strength is $k_{\rm pot} \simeq 10^{-6} N/m$, the viscosity of water is $\eta \simeq 10^{-3} Ns/m^2$ and typical flow velocities in microfluidic environments are of the order of $u_0(d_w) \simeq 10^{-6} m/s$. Using these values one obtains

$$\frac{\Delta_b}{a} \simeq \frac{\eta u_0(d_w)}{k_{\rm pot}} \simeq 10^{-3}\,, \tag{23}$$

which might be below the currently possible experimental resolution. However, Δ_b can be enhanced by using a liquid with a higher viscosity than water as for example glycerol with $\eta \simeq 1 Ns/m^2$, but then the maximum attainable flow velocities may be smaller. Furthermore, the effect can be amplified by placing several beads in a row and measuring the deflection of the final bead. An amplification of Δ_b by about 10% can be reached by using five beads in a row. Compared to this estimate, sedimentation experiments close to a wall, as described in section V, seem to be more appropriate for the detection of the wall-induced HI effects.

The results discussed until now apply to linear shear flow, but the most important property, that the streamlines are parallel to the wall, is also shared by other flow profiles like plane Poiseuille flow. The spatially varying shear rate in Poiseuille flow causes higher order effects, but the major results presented here remain qualitatively valid to Poiseuille flow, as well.

IV. APPLICATIONS TO SEMIFLEXIBLE BEAD-SPRING CHAINS

In this section we explore applications of the wall-mediated HI effects of tethered semiflexible bead-spring models in a flow and fixed near a wall in Sec. IV A or grafted to the boundary in Sec. IV B.

A. Polymer model fixed near a wall

Polymers tethered with one end in a uniform flow is a model system for exploring the importance of HI along polymers at various stages of its flow-induced conformations [51–56]. Here we consider a semiflexible bead-spring polymer model with its first bead tethered at a distance d_w from a wall as shown in Fig. 11 and we explore the importance of wall-induced hydrodynamic interaction effects.

The stationary chain conformation in shear flow is again determined via Eq. (10) by using the potential energy for the elastic forces along the polymer

$$V = \frac{k_{\rm trap}}{2}(\mathbf{r}_1 - \mathbf{r}_{\rm trap})^2 + \sum_{i=1}^{N-1} \frac{k_{\rm str}}{2}(|\mathbf{r}_i - \mathbf{r}_{i+1}| - d_{\rm n})^2 + \sum_{i=2}^{N-1} \frac{k_{\rm bend}}{2} \ln\left(1 + \cos\chi_i\right), \tag{24}$$

with $\mathbf{r}_{\rm trap} = (0, 0, d_w)$ the location of the minimum of the trap potential of strength $k_{\rm trap} = 1$. $k_{\rm str} = 500$ is the stretching stiffness of the springs and $d_n = 5a$ is the equilibrium distance between neighboring beads. The bending stiffness is $k_{\rm bend} = 100$ and the bending angle at the i-th bead is $\chi_i = \arccos\left[(\mathbf{r}_i - \mathbf{r}_{i-1}) \cdot (\mathbf{r}_{i+1} - \mathbf{r}_i)\right]$. The distances between the beads along the chain are practically fixed on the time scale of the bending dynamics, which can be seen by the ratio of the relaxation times of stretching and bending: $\tau_{\rm str}/\tau_{\rm bend} = 2k_{\rm bend}/(d_{\rm n}^2 k_{\rm str}) \simeq 1/60$.

In the following we consider chains consisting of $N = 10$ beads as an example.

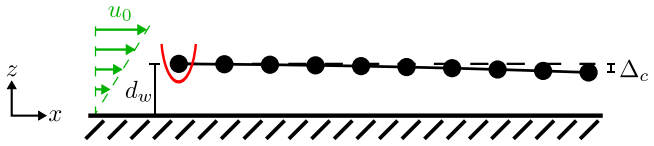

FIG. 11. A semiflexible chain, fixed with one end at a distance d_w from a wall and exposed to a linear shear flow, is attracted towards the wall with its free end by a distance Δ_c. This shift depends on d_w as shown in Fig. 12. For the displayed configuration the parameters are $d_w = 5.5a$ and $u_0(d_w) = 0.004$.

In an unbounded fluid the tethered polymer would assume a straight conformation, parallel to the streamlines of the external flow. However, in the presence of a wall the free end of the chain is attracted via the wall-induced HI. This is similar to the bead attraction downstream investigated in the previous section and to the hydrodynamically induced attraction between two tethered polymers in plug flow and Brownian motion as described in Ref. [39]. A measure of the effective wall attraction is the deflection $\Delta_c = d_w - z_N$ of the N-th bead towards the wall, which is shown in Fig. 11 for $d_w = 5.5a$ and the flow profile (22) with $u_0(d_w) = 0.004$.

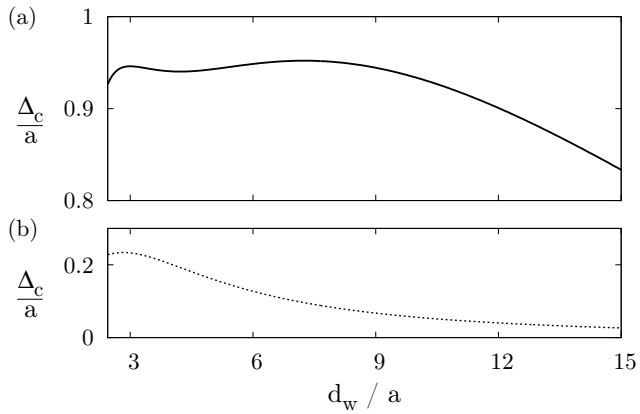

FIG. 12. The deflection Δ_c of the free end of a tethered chain consisting of $N = 10$ beads (cf. Fig. 11) is shown as a function of the distance d_w to the wall for the flow field given by Eq. (22) with $u_0(d_w) = 0.004$. For the solid line in (a) the wall-mediated HI between all beads is taken into account. The dotted line in (b) corresponds to the model assumption where the wall-induced HI has only been taken into account for nearest neighbors and has been neglected otherwise.

Δ_c is plotted as a function of the wall distance in Fig. 12 for the constant flow velocity $u_0(d_w) = 0.004$ at $z = d_w$. The solid line in part (a) describes the case wherein the wall-mediated HI between all beads is taken into account. In contrast to the curve for two beads in Fig. 8, it displays two maxima and decreases monotonically afterwards. The first maximum of $\Delta_c(d_w)$ at $d_w \simeq 3a$ is mainly caused by the wall-induced HI between nearest-neighbor beads along the chain. In order to substantiate this interpretation, we plot $\Delta_c(d_w)$ in Fig. 12(b) for the model situation where the wall-mediated HI is only taken into account between nearest neighbor beads. In this case, the magnitude of $\Delta_c(d_w)$ is much smaller and has indeed only one maximum at $d_w \simeq 2.9a$. The small shift between this maximum and the first maximum of the curve in Fig. 12(a) is caused by the boundary-induced HI between beads which are further apart. The second maximum at $d_w = 7.3a$ in Fig. 12(a) is also a result of hydrodynamic bead-bead interactions via the wall over larger distances than nearest neighbors.

Besides the deflection of the free end, the chain exhibits also a small curvature. This can be explained as follows: The trapping potential prevents the fixed end of the chain from moving away from the wall. On the other hand each bead is driven to the wall due to the flow perturbations from all its neighbors upstream. Therefore, the beads closer to the free end are increasingly attracted towards the wall, which leads to a slight bending of the chain.

B. Perpendicularly anchored semiflexible chains in flow

As wall-grafted polymers are relevant in several applications [27] we investigate the influence of the boundary on the behavior of semiflexible chains, which are perpendicularly grafted to a wall and exposed to a shear flow as shown in Fig. 13.

For our model calculations we use a potential energy describing the bending and stretching of the N_c chains as given by

$$V = \sum_{j=1}^{N_c} V^j \quad \text{with} \tag{25}$$

$$V^j = \sum_{i=1}^{N-1} \frac{k_{\rm str}}{2} (|\mathbf{r}_i^j - \mathbf{r}_{i+1}^j| - d_{\rm n})^2 + \sum_{i=0}^{N-1} \frac{k_{\rm bend}}{2} \ln(1 + \cos\chi_i^j)\,. \tag{26}$$

Here $\mathbf{r}_i^j$ and χ_i^j are the position vector and the bending angle of the i-th bead in the j-th chain. The constants $k_{\rm str}$, $d_{\rm n}$ and $k_{\rm bend}$ have the same values as in the previous subsection, but the chains are now composed of $N = 9$ beads. However, the second sum in Eq. 26 starts with $i = 0$ and therefore includes additional bending contributions at the boundary in order to ensure that the chain relaxes back to an orientation perpendicular to the wall after switching off the flow.

A single chain is bent towards the flow direction until the forces exerted on the beads due to the external drag are balanced by the stretching and bending forces according to Eq. (26). If the flow velocity is very large, the chain even goes beyond the alignment with the flow lines and bends towards the wall similar to the results presented in Sec. IV A.

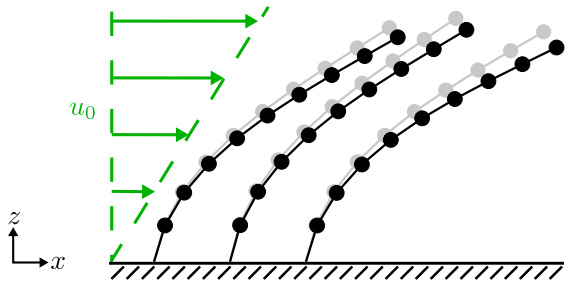

FIG. 13. Three bead-spring chains, which are perpendicularly anchored at a boundary and exposed to a linear shear flow. For the grey conformation the wall-mediated HI is neglected and only the bulk HI effects are taken into account.

For three chains, which are perpendicularly grafted to a wall, Fig. 13 shows the steady state chain conformations for the case in which the wall-mediated contributions to the HI are neglected (grey) and for the case in which the HI via the boundary is completely included (black). In the free draining limit, where the HI between the beads are disregarded, the three perpendicularly anchored polymers would be bent identically by the flow. If only the effects of bulk HI are taken into account, the outer polymers perturb the flow in such a way, that the middle polymer experiences a smaller drag force. Hence, the first and the last polymer, *i.e.* the left and the right one in Fig. 13, are bent almost identically, while the one in between is bent less strongly, which is indicated by the grey configuration in Fig. 13.

Similar to the results from the previous subsection, the wall-mediated HI leads to a stronger bending of the chains towards the wall, which is displayed by the deviation of the black chain configurations from the grey ones in Fig. 13. This attractive effect increases for chains which lie further downstream, because the wall-attraction of each chain bead is enhanced by its neighbors upstream as described in Sec. IV A. The screening effect for the middle chain due to the interactions in the bulk is therefore superimposed by the wall-induced effect.

Consequently, the wall-mediated HI along this semiflexible brush leads to a stronger bending of the chains and thus to a reduction of the brush height. So the effective diameter of a polymer-grafted tube is increased and the flow resistance of the grafted chains is reduced, which might be interesting for studies on wall-grafted brushes of semiflexible polymers or for a wall decorated by thin flexible pillars.

V. CONCLUSIONS

In our investigations of wall-induced effects on the statics and the dynamics of hydrodynamically interacting particles we first calculated the streamline deformation around a single trapped point-like particle close to a wall in order to develop a qualitative picture about the particle-particle interaction near a wall. It was shown how the deformations of the flow lines around a fixed particle allow an estimation of the direction of the force acting on a nearby second particle, which was confirmed by numerical calculations.

For two or three beads being dragged parallel to a wall, a scenario with resemblance to sedimenting particles under gravity, it was shown that the beads always migrate away from the wall. The origin of this behavior is due to the interplay between effects from the bulk and the boundary, and it is similar to the lift force discussed for vesicles and polymers [11, 12, 17, 34].

The analysis of the configurations of two beads, which are trapped by harmonic potentials close to a wall and exposed to an external shear flow, provided further insight about the hydrodynamically mediated particle wall interaction. We found a repulsion from the wall for the particle upstream and an attraction towards the boundary for the one downstream. Varying the particle-wall distance and the particle-particle distance a characteristic maximum in the deflection of the downstream particle was found, which could be described also analytically giving further insight on the parameter dependence of this phenomenon. The behavior obtained for two point-like particles was confirmed by using the complementary method of Fluid Particle Dynamics [45, 46], which accounts for the finite particle radii and the effects of particle rotation on the hydrodynamic particle-particle interaction.

As an application of the basic effects found for the two-bead configuration, we investigated a semiflexible bead-spring chain, where one end is held in a linear shear flow at a distance d_w from the boundary. The chain is attracted towards the boundary as a function of d_w and we identified the wall-induced contributions to the HI as the source for this behavior. The phenomenon is related to a recent study on the flow induced polymer-polymer attraction [39] mediated through inter-chain HI, where the second polymer causes very similar effects as the boundary in this work. Both are examples of hydrodynamically induced particle-particle attraction, which has recently been found for rotors as well [38].

What is more, three perpendicularly anchored semiflexible bead-spring chains were investigated as a simple model for a polymer brush and their response to an external linear shear flow was obtained. It was found , that wall-effects cause a stronger effective attraction towards the wall for the polymers downstream than for the ones upstream. Whether three semiflexible polymers, perpendicularly anchored at a wall, but not along a line, and of different length, have also the propensity to oscillatory motion as reported for three beads in shear flow in

Ref. [35], is an interesting further question.

While our analysis in this work is exclusively used for a linear shear flow as external stimulus, we nonetheless expect a similar qualitative behavior for other flow profiles with parallel streamlines. The reason is, that the deformations of the streamlines near walls as shown in Fig. 1 are in general the same for other laminar flow profiles with parallel streamlines.

Our results may be tested by different experiments. A first one would be to measure the wall-induced displacement of an array of beads trapped close to wall by laser tweezers while imposing an external flow similar to the setups shown in Fig. 7 and Fig. 11. A variation of the above setup may be to measure the deflection of a cantilever in proximity of a wall and exposed to a flow as illustrated for a model polymer in Sec. IV A.

Another alternative to probe our findings is to line up two particles in a row close to the wall of a container, extended in its vertical direction, and to track the trajectories of the two sedimenting particles. According to our predictions, the particle moving in front should be repelled from the wall whereas the particle behind should at first be attracted. As soon as the connection vector between the particles becomes sufficiently oblique with respect to the boundary, the bulk effect is expected to become dominant, so that both beads are carried both away from the wall.

ACKNOWLEDGMENTS

Inspiring discussions with Diego Kienle and Chaouqi Misbah are acknowledged. This work has been supported by the German science foundation (through FOR 608 and SPP 1164) and by the Bayerisch-Französisches Hochschulzentrum (BFHZ).

[1] J. Happel and H. Brenner, *Low Reynolds Number Hydrodynamics* (Prentice-Hall, Englewood Cliffs, 1981).
[2] W. B. Russel, D. A. Saville, and W. R. Showalter, *Colloidal Dispersions* (Cambridge University Press, Cambridge, 1989).
[3] J. K. G. Dhont, *An Introduction to dynamics of colloids* (Elsevier, Amsterdam, 1996).
[4] L. G. Leal, *Advanced Transport Phenomena*, (Cambridge University Press, Cambridge, 2007).
[5] G. Segré and A. Silberberg, "Radial Poiseuille flow of suspensions," Nature **189**, 209 (1961).
[6] G. Segré and A. Silberberg, "Behavior of macroscopic rigid spheres in Poiseuille flow. Part 1. Determination of local concentration by statistical analysis of particle passages through crossed light beams," J. Fluid Mech. **14**, 115 (1962).
[7] L. G. Leal, "Particle motions in a viscous fluid," Ann. Rev. Fluid Mech. **12**, 435 (1980).
[8] J. A. Schonberg and E. J. Hinch, "Inertial migration of solid particles in Poiseuille flow - I. Theory," J. Fluid Mech. **203**, 517 (1989).
[9] B. H. Yang, J. Wang, D. D. Joseph, H. H. Hu, T. W. Pan, and R. Glowinski, "Migration of a sphere in tube flow," J. Fluid Mech. **540**, 109 (2005).
[10] D. Di Carlo, J. F. Edd, K. J. Humphry, H. A. Stone, and M. Toner, "Particle segregation and dynamics of confined flows," Phys. Rev. Lett. **102**, 094503 (2009).
[11] U. Seifert, "Hydrodynamic lift on bound vesicles," Phys. Rev. Lett. **83**, 876 (1999).
[12] I. Cantat and C. Misbah, "Lift force and dynamically unbinding of adhering vesicles under shear flow," Phys. Rev. Lett. **83**, 880 (1999).
[13] M. Abkarian, C. Lartigue, and A. Viallat, "Tank Treading and unbinding of deformable vesicles in shear flow: Determination of the lift force," Phys. Rev. Lett. **88**, 068102 (2002).
[14] B. Kaoui, G. H. Ristow, I. Cantat, C. Misbah, and W. Zimmermann, "Lateral migration of a two-dimensional vesicle in unbounded Poiseuille flow," Phys. Rev. E **77**, 021903 (2008).
[15] G. Coupier, B. Kaoui, T. Podgorski, and C. Misbah, "Noninertial lateral migration of vesicles in bounded Poiseuille flow," Phys. Fluids **20**, 111702 (2008).
[16] U. S. Agarwal, A. Dutta, and R. A. Mashelkar, "Migration of macromolecules under flow: The physical origin and engineering implications," Chem. Eng. Sci. **49**, 1693 (1994).
[17] R. M. Jendrejack, D. C. Schwartz, J. J. de Pablo, and M. D. Graham, "Shear-induced migration in flowing polymer solutions: Simulation of long-chain DNA in microchannels," J. Chem. Phys. **120**, 2513 (2004).
[18] J. P Hernández-Ortiz and H. Ma and J. J. de Pablo, and M. D. Graham, "Cross-streamline migration in confined flowing polymer solutions: Theory and simulation," Phys. Fluids **18**, 123101 (2006).
[19] M. Graham, "Fluid dynamics of dissolved polymer molecules in confined geometries," Annu. Rev. Fluid Mech. **43**, 273 (2011).
[20] R. Chelakkot, R. G. Winkler, and G. Gompper, "Migration of semiflexible polymers in microcapillary flow," EPL **91**, 14001 (2010).
[21] A. F. Fortes, D. D. Joseph, and T. S. Lundgren, "Nonlinear mechanics of fluidization of beds of spherical particles," J. Fluid Mech. **177**, 467 (1987).
[22] E. Kuusela, J. M. Lahtinen, and T. Ala-Nissila, "Sedimentation dynamics of spherical particles in confined geometries," Phys. Rev. E **69**, 066310 (2004).
[23] E. Lauga and T. R. Powers, "The hydrodynamics of swimming microorganisms," Rep. Prog. Phys. **72**, 096601 (2009).
[24] A. P. Berke, L. Turner, H. C. Berg, and E. Lauga, "Hydrodynamic attraction of swimming microorganisms by surfaces," Phys. Rev. Lett. **101**, 038102 (2008).
[25] S. Minko, "Responsive polymer brushes," J. Macromol. Sci. C: Pol. Rev., **46**, 397 (2006).
[26] S. P. Adiga and D. W. Brenner, "Flow control through polymer-grafted smart nanofluidic channels: Molecular dynamics simulations," Nanolett. **5**, 2509 (2005).

[27] P. Uhlmann, H. Merlitz, J. U. Sommer, and M. Stamm, "Polymer brushes for surface tuning," Macromol. Rapid Comm. **30**, 732 (2009).
[28] P. S. Doyle, B. Ladoux, and J.-L. Viovy, "Dynamics of a tethered polymer in shear flow," Phys. Rev. Lett. **84**, 4769 (2000).
[29] C. M. Schroeder, R. E. Teixeira, E. S. G. Shaqfeh, and S. Chu, "Characteristic periodic motion of polymers in shear flow," Phys. Rev. Lett. **95**, 018301 (2005).
[30] R. Delgado-Buscalioni, "Cyclic motion of a grafted polymer under shear flow," Phys. Rev. Lett. **96**, 088303 (2006).
[31] C. A. Lueth and E. S. G. Shaqfeh, "Experimental and numerical studies of tethered DNA shear dynamics in flow-gradient plane," Macromolecules **42**, 9170 (2009).
[32] Y. Zhang, A. Donev, T. Weisgraber, B. J. Alder, M. D. Graham, and J. J. de Pablo, "Tethered DNA dynamics in shear flow," J. Chem. Phys. **130**, 234902 (2009).
[33] G. L. He, R. Messina, H. Löwen, A. Kiriy, V. Bocharova, and M. Stamm, "Shear-induced stretching of adsorbed polymer chains," Soft Matter **5**, 3014 (2009).
[34] C. E. Sing and A. Alexander-Katz, "Non-monotonic hydrodynamic lift force on highly extended polymers near surfaces," EPL **95**, 48001 (2011).
[35] L. Holzer and W. Zimmermann, "Particles held by springs in a linear shear flow exhibit oscillatory motion," Phys. Rev. E **73**, 060801 (R) (2006).
[36] A. Carlsson, F. Lundell, and L. Söderberg, "Fiber orientation control related to papermaking," J. Fluids Eng. **129**, 457 (2007).
[37] R. E. Caflisch, C. Lim, J. H. C. Luke, and A. S. Sangami, "Periodic solutions for three sedimenting spheres ," Phys. Fluids **31**, 3175 (1988).
[38] S. Schreiber, T. Fischer, and W. Zimmermann, "Hydrodynamic attraction and repulsion between asymmetric rotors," New J. Phys. **12**, 073017 (2010).
[39] D. Kienle, R. Rzehak, and W. Zimmermann, "Identifying hydrodynamic interaction effects in tethered polymers in uniform flow," Phys. Rev. E **83**, 062802 (2011).
[40] I. E. Zarraga and D. T. Leighton, "Measurement of an unexpectedly large shear-induced self-diffusivity in a dilute suspension of spheres," Phys. Fluids **14**, 2194 (2002).
[41] M. Zurita-Gotor, J. Blawzdziewicz, and E. Wajnryb, "Swapping trajectories: a new wall-induced cross-streamline particle migration mechanism in a dilute suspension of spheres," J. Fluid Mech. **592**, 447 (2007).
[42] J. R. Blake, "A note on the image system for a stokeslet in a no-slip boundary," Proc. Camb. Phil. Soc. **70**, 303 (1971).
[43] B. Cichocki, R. B. Jones, R. Kutteh, and E. Wajnryb, "Friction and mobility for colloidal spheres in Stokes flow near a boundary: The multipole method and applications," J. Chem. Phys. **117**, 2548 (2000).
[44] J. W. Swan and J. F. Brady, "Simulation of hydrodynamically interacting particles near a no-slip boundary," Phys. Fluids **19**, 113306 (2007).
[45] H. Tanaka and T. Araki, "Simulation method of colloidal suspensions with hydrodynamic interactions: Fluid particle dynamics," Phys. Rev. Lett. **85**, 1338 (2000).
[46] P. Peyla, "Rheology and dynamics of a deformable object in a microfluidic configuration: a numerical study," EPL **80**, 34001 (2007); Y. Davit and P. Peyla, "Intriguing viscosity effects in confined suspensions : a numerical study," EPL **83**, 64001 (2008); Jibuti, S. Rafai and P. Peyla, "Suspensions with a tunable effective viscosity: a numerical study," J. Fluid Mech. **693**, 345 (2012).
[47] T. Naik, E. Longmire, and S. Mantell, "Dynamic response of a cantilever in liquid near a solid wall," Sensors and Actuators, **102**, 240 (2007).
[48] A. J. Goldman, R. G. Cox, and H. Brenner, "The slow motion of two identical arbitrarily oriented spheres through a viscous fluid," Chem. Eng. Sci. **21**, 1151 (1966).
[49] A. J. Goldman, R. G. Cox, and H. Brenner, "Slow viscous motion of a sphere parallel to a plane wall I Motion through a quiescent fluid," Chem. Eng. Sci **22**, 637 (1967).
[50] A. J. Goldman, R. G. Cox, and H. Brenner, "Slow viscous motion of a sphere parallel to a plane wall II Couette flow," Chem. Eng. Sci **22**, 653 (1967).
[51] T. T. Perkins, D. E. Smith, R. Larson, and S. Chu, "Stretching of a Single Tethered Polymer in a Uniform Flow," Science **268**, 83 (1995).
[52] R. G. Larson, T. T. Perkins, D. E. Smith, and S. Chu, "Hydrodynamics of a DNA molecule in a flow field," Phys. Rev. E **55**, 1794 (1997).
[53] R. Rzehak, D. Kienle, T. Kawakatsu, and W. Zimmermann, "Partial draining effect of a tethered polymer in flow," Europhys. Lett. **46**, 821 (1999).
[54] R. Rzehak, W. Kromen, T. Kawakatsu, and W. Zimmermann, "Deformations of tethered polymers in uniform flow," Eur. Phys. J. E. **2**, 3 (2000).
[55] F. Brochard-Wyart, "Deformations of one tethered chain in strong flows," Europhys. Lett. **23**, 105 (1993).
[56] D. Kienle and W. Zimmermann, "F-Shell Blob-Modell for a Tethered Polymer in Strong Flows," Macromolecules **34**, 9173 (2001).